

Far-infrared-driven electron-hole correlations in a quantum dot with an internal tunneling barrier

Roger Sakhel, Lars Jönsson, and John W. Wilkins

Department of Physics, The Ohio State University, Columbus, Ohio 43210-1106

(Received 18 December 2000; published 27 September 2001)

Laser excited and FIR-driven, time-dependent electron-hole correlations in a prototypical GaAs quantum dot with an internal AlGaAs tunneling barrier are studied by numerical propagation of the time-dependent Schrödinger equation. The dimensions of the dot are $13 \times 25 \times 25 \text{ nm}^3$ (denoted x , y , and z directions, respectively). The width of the symmetrically placed barrier in the x direction varies between 1 and 4 nm. The simulations, including a screened Coulomb interaction, time-propagates the electron-hole (exciton) wave function within the effective mass approximation. The Coulomb correlations are treated within the time-dependent configuration-interaction method. The hole mass is chosen to be heavy along the growth direction (x) and light in the lateral directions. The presence of the barrier allows the energy splittings of the excited states to be tuned for optimal correlation effects. Three cases illustrate how sequences of NIR and FIR pulses can excite and probe coherent correlation effects. Case I: A single FIR-coupled dark eigenstate can be used to modulate correlation induced beatings in a pair of optically excited eigenstates, but the beating is not significantly transferred into the dark state. Case II: With appropriate FIR pulse widths and center frequencies, a coherent optical excitation in a pair of correlation split states can be transferred unchanged into and out of a pair of optically dark states split by similar correlations. Case III: Correlations open new optical pathways that, for example, allow FIR pulses polarized in the x direction to transfer an excitonic excitation in x to an excitation in the perpendicular y and z directions.

DOI: 10.1103/PhysRevB.64.155322

PACS number(s): 78.67.Hc, 73.21.La, 71.35.-y

I. INTRODUCTION

A nanoscale semiconductor quantum dot of typical dimension d of the order of an exciton (electron-hole pair) diameter (20 nm in GaAs) has unique optical properties due to the interplay between confinement and correlation.¹⁻⁶ The Coulomb interaction between the electron and the hole forms the exciton—a hydrogenlike system with radius a_{ex} scaled by the dielectric constant of the semiconductor and the effective masses.⁷ The interplay between confinement and correlation is less important for both larger ($d \gg a_{ex}$) and smaller dots ($d \ll a_{ex}$). For large dots, confinement effects are negligible, whereas for small dots confinement effects dominate and the correlations are weak. The typical energy scale for Coulomb interactions and kinetic excitations in a dot with $d \sim a_{ex}$ is 1–100 meV.

If an internal tunneling barrier is introduced in the quantum dot, the typical energy splitting caused by the barrier is of the order of tens of meV. The tunneling dynamics is therefore strongly coupled to the kinetic and correlation dynamics. The resulting strong coupling between kinetic, correlation, and tunneling effects can be probed by short near infrared (NIR) pulses, with spectral *widths* of the order of the characteristic excitation energies (1–100 meV), and by far infrared (FIR) pulses with frequencies that can resonantly couple the excited states. That is, NIR pulses can be used to set up coherent beatings given by the energy splittings, while the FIR pulses can be used to make population transfers. In previous work, we have shown how NIR pulses can be used to excite and probe time-dependent correlations for an exciton⁵ and for a biexciton⁶ in a single GaAs model quantum dot. These results were obtained by numerical time propagation of the many-electron Schrödinger equation including both the Coulomb interaction between particles and

their interaction with NIR and FIR laser pulses.

In this paper, we introduce an AlGaAs tunneling barrier in the dot and show how the barrier width can be used to tune the correlation effects and how FIR laser pulses can be used to probe the coherent time-dependent correlations in states that are not accessible by direct optical excitation. For example, using sequences of NIR and FIR pulses we show that coherent optical excitations can be transferred between radiative and dark pairs of excited states, and that new FIR pathways are created by the Coulomb correlations. Although we throughout use the term “internal barrier,” our model is also representative of two coupled quantum dots. However, our choice of materials is based on the notion of an epitaxially grown internal barrier, with the prototypical materials being an AlGaAs barrier and GaAs wells between AlGaAs outer walls. For coupled quantum dots, the prototypical case would be stacked self-assembled InAs pyramids embedded in GaAs. In addition, since the simulations use a simplified model, the particular dot dimensions or pulse parameters are not essential. Our goal is to describe different correlation-induced effects that can be optically excited and probed and that we judge to be qualitatively similar to those expected of more realistic dots.

Other theoretical work on nanoscale semiconductor structures has focused primarily on the stationary properties. Bryant applied configuration-interaction methods to obtain the correlated bound states of excitons in quantum dots, including the tunneling between coupled dots.^{3,8,9} This has been followed by several other calculations of exchange and correlation in quantum dots.¹⁰⁻¹⁶ Optical excitations, including both interband and intersublevel transitions, have also been studied extensively. For example, $\mathbf{k} \cdot \mathbf{p}$ theory, pseudopotential methods, and tight-binding models have been used to calculate the optical absorption spectra.¹¹⁻²³ A study of the

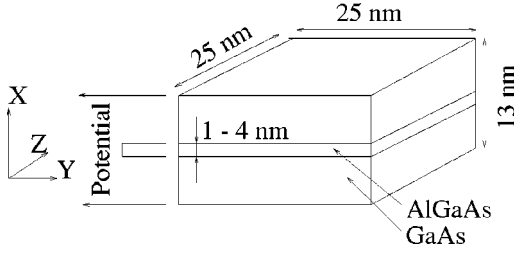


FIG. 1. Our model: a GaAs dot with an internal AlGaAs tunneling barrier placed symmetrically in the dot. The tunneling barrier has a finite potential for the electron and the hole ($V_e = 0.3$ eV and $V_h = 0.1$ eV). The potential of the outer walls is infinite. The hole mass is heavy along the growth direction (x) and light in the lateral directions.

intersublevel absorption in coupled dots verified that the absorption is strongly affected by the distance between the dots.²⁴ The effect of the electron number on the FIR absorption spectrum has also been investigated.^{25,26}

Experimental work on nanoscale semiconductor structures usually involves excitation by NIR and FIR pulses. The exciton recombination process occurs on a time scale of a few hundred picoseconds to nanoseconds, which is easily accessible to time-resolved photoluminescence. Photoluminescence experiments have been used to show the presence of excitons in a variety of dots via their sharp spectral features.^{27–33} For example, individual InAs quantum dots embedded in GaAs have been investigated using optical spectroscopy at different temperatures and excitation intensities.²¹ The effect of changing the intersublevel spacing in self-assembled InAs/GaAs dots has also been investigated by photoluminescence studies. The level spacing was modified by adjusting the growth temperature,^{34–37} or the layering thickness.³⁸ Far infrared absorption in self-assembled quantum dots has shown that the electronic coupling between the dot states leads to intersublevel absorption at THz frequencies.^{39,40} Third harmonic generation associated with intersublevel transitions, and in-plane polarized intersublevel absorption have also been observed in self-assembled InAs/GaAs dots.^{41,42}

II. THEORY

A. Our model

Our model, shown in Fig. 1, is a prototypical GaAs quantum dot with an internal AlGaAs tunneling barrier of finite height and adjustable width. For simplicity, the potential of the outer walls is infinite. The dimensions of the model are $13 \times 25 \times 25$ nm³ (denoted x , y , and z directions, respectively). GaAs has a direct band gap of 1.5 eV from a p -type valence band to an s -type conduction band, and a dielectric constant $\epsilon = 13$. Within the effective-mass approximation, we treat a single exciton confined in the dot. The hole states are fourfold degenerate at the Γ point with different masses for the hole along the growth direction (x axis) and lateral directions.⁷ According to the Luttinger model, the hole mass depends on the choice of the quantization axis.^{43–45} Since our dot has equal lateral dimensions and a tunneling barrier

along the shorter x dimension, the convenient choice of the quantization axis is along x . The heavy hole along x has angular momentum $J_x = \pm 3/2$ and the light hole has $J_x = \pm 1/2$. We choose the hole that is heavy along the growth direction and hence light in the lateral directions. That choice gives the lowest energies, and the electron and hole have approximately equal masses in the lateral directions, which gives an optimal interplay between kinetic and correlation effects. The masses used are $m_{hh} = 0.5m_0$, $m_{lh} = 0.08m_0$, and $m_e = 0.07m_0$, where m_0 is the free-electron mass.

The exciton Hamiltonian has the form (in atomic units)

$$\begin{aligned} H = & -\frac{1}{2m_{hh}} \frac{d^2}{dx_h^2} - \frac{1}{2m_{lh}} \left(\frac{d^2}{dy_h^2} + \frac{d^2}{dz_h^2} \right) \\ & - \frac{1}{2m_e} \left(\frac{d^2}{dx_e^2} + \frac{d^2}{dy_e^2} + \frac{d^2}{dz_e^2} \right) + V_h(x_h) + V_e(x_e) \\ & - \frac{1}{\epsilon |\mathbf{r}_e - \mathbf{r}_h|} + \hat{\mathbf{D}}_{\text{inter}} \cdot \mathbf{E}_{\text{NIR}}(t) + \hat{\mathbf{D}}_{\text{intersub}} \cdot \mathbf{E}_{\text{FIR}}(t), \quad (1) \end{aligned}$$

where the first two terms represent the kinetic energies of the hole in the growth and the lateral directions, respectively, and the third term is the kinetic energy of the electron. The hole barrier $V_h(x_h)$ is given by

$$\begin{aligned} V_h(x_h) = & \begin{cases} 0.0 \text{ eV} & \text{for } -L_x/2 < x_h < -a/2 \text{ and } a/2 < x_h < L_x/2 \\ 0.1 \text{ eV} & \text{for } -a/2 < x_h < a/2 \end{cases} \quad (2) \end{aligned}$$

and the electron barrier $V_e(x_e)$ by

$$\begin{aligned} V_e(x_e) = & \begin{cases} 0.0 \text{ eV} & \text{for } -L_x/2 < x_e < -a/2 \text{ and } a/2 < x_e < L_x/2 \\ 0.3 \text{ eV} & \text{for } -a/2 < x_e < a/2, \end{cases} \quad (3) \end{aligned}$$

where a is the barrier width, and L_x is the length in x . The sixth term in Eq. (1) is the screened Coulomb interaction. In the last two terms, $\hat{\mathbf{D}}_{\text{inter}}$ and $\hat{\mathbf{D}}_{\text{intersub}}$ are the interband and intersublevel dipole operators, respectively, and \mathbf{E}_{NIR} and \mathbf{E}_{FIR} are the NIR and FIR laser fields, respectively. We take the direction of incidence of the NIR pulses and the polarization for the FIR pulses along the x axis. Therefore the intersublevel transitions occur only in that direction.

The barrier heights above were chosen by the following considerations. In a realistic system, the barrier height depends on the aluminum concentration x of the $\text{Al}_x\text{Ga}_{1-x}\text{As}$ barrier material which has a direct band gap at room temperature.^{46,47} The GaAs direct band gap 1.5 eV that we use in our model is for 0 K. The temperature-dependent GaAs band gap changes by about 10% between 0 and 300 K (1.4 eV at 300 K).^{47,48} For $\text{Al}_{0.3}\text{Ga}_{0.7}\text{As}$ at room temperature the gap was determined experimentally to be 1.8 eV.⁴⁹ Assuming approximately the same temperature dependence as for GaAs and taking into account the (65–35% rule),^{45,50,51}

we find the potential barrier heights $V_e=0.26$ eV and $V_h=0.14$ eV for 0 K. Based on these estimates we choose $V_e=0.3$ eV and $V_h=0.1$ eV in our model system.

The symmetrically placed barrier along the x axis leads to orbitals of well-defined parity, and the infinite potentials in the lateral directions ensure sinusoidal orbitals. We restrict our attention to the electron and hole energies below the barrier because we are interested in the tunneling states. Using Eqs. (2) and (3) as well as the values for m_{hh} and m_e mentioned previously, the heavy hole and electron energy levels are found by the standard procedure of matching the wave function and its derivative just inside and outside the barrier. The resulting energy-dependent matching equation for each parity is solved by a bisection search.⁵²

We want to simulate the interaction of an exciton with both NIR and FIR pulses. There are two possible types of excitations: interband and intersublevel, which are induced by NIR and FIR pulses, respectively. Both kinds of pulses are able to excite and probe correlation induced optical effects. NIR pulses create an exciton in an initially empty dot, and FIR pulses drive the intersublevel transitions. In our model, the FIR pulses couple to the intersublevel dipole matrix elements in the x direction. Further, the NIR pulses are incident in the x direction, and we choose their polarization to be right circular. We could equally well have chosen the opposite circular polarization or linearly polarized NIR pulses with no qualitative differences in the results. This is true because we are dealing with only one exciton. In contrast, for biexcitons, for example, circular and linear polarization can give qualitatively different effects.⁵³

B. Selection rules and Coulomb coupling

The selection rules follow from the functional form of the single-particle orbitals. These orbitals are given by

$$|n_x, n_y, n_z\rangle \propto \phi_{n_x} \sin(n_y \pi y / L_y) \sin(n_z \pi z / L_z), \quad (4)$$

where ϕ_{n_x} are the even and odd orbitals in the x direction, n_x , n_y , and n_z are positive quantum numbers, and L_y , L_z are the lateral lengths ($L_y=L_z=25$ nm). The single-particle wave functions consist of a fast-varying Bloch function and these slowly varying envelope functions.^{44–46,54} The interband transitions either create or recombine an electron-hole pair in an s -like conduction band and a p -like valence band. The dipole selection rule is fulfilled by the p to s transition in the Bloch part of the wave function. The envelope part contributes a factor equal to the overlap between the electron and hole orbitals. This factor due to the overlap of the electron and hole orbitals yields the interband selection rule $(n_x, n_y, n_z)_{elec} = (n_x, n_y, n_z)_{hole}$.^{44–46,54} This rule is valid for $n_x \leq 2$ and all n_y, n_z . However, due to the different potentials and masses for the electron and hole, there is, for example, some overlap between the $n_x=1$ electron and $n_x=3$ hole orbital. For example, for a barrier width of 2.8 nm the overlap is 18%. In this paper, we will, for simplicity, use the term “dark” for all the transitions that do not fulfill the above selection rule (forbidden transitions).

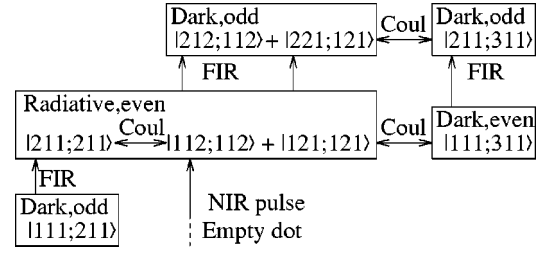


FIG. 2. Illustration of the coupling scheme in our model dot. We use the notation $|n_x n_y n_z (elec); n_x n_y n_z (hole)\rangle$ for the determinants, where n_x , n_y , and n_z are positive quantum numbers. The radiative determinants of even overall parity satisfy the interband selection rule, and can be optically excited from an empty dot. As seen in the figure, the presence of the Coulomb interaction causes different types of coupling. The $|112;112\rangle$ and $|121;121\rangle$ radiative determinants couple to the $|211;211\rangle$ radiative determinant. The Coulomb interaction also couples the nonradiative $|111;311\rangle$ determinant to the radiative ones, and the odd-parity nonradiative $|212;112\rangle$ and $|221;121\rangle$ determinants to the nonradiative $|211;311\rangle$ determinant. An FIR induces a transfer between determinants of different parity in x , by changing n_x between 1 and 2.

The exciton basis states are products of single-particle orbitals. Although we only have single-exciton states, and therefore have only products and no proper Slater determinants, we call the exciton basis states “determinants” throughout this paper. The determinants that satisfy the interband selection rule have an even overall parity and are optically active (radiative). Determinants which do not satisfy that selection rule are optically dark (nonradiative). The intersublevel transitions occur between levels of the same particle and follow the normal dipole selection rules for the envelope functions. That is, *even parity* \leftrightarrow *odd parity* in the x direction.

In the growth direction, the orbitals have different functional forms inside and outside the barrier. Within the barrier, the orbitals have a hyperbolic sine and a hyperbolic cosine dependence for the odd and even parity cases, respectively. Outside the barrier, they have sinusoidal behavior. The particle masses and barrier heights chosen yield an upper orbital limit for n_x which is two for the electron and four for the heavy hole. In the lateral directions, we typically choose the upper limit to be two for n_y and n_z . For all the results presented in this paper, we have verified that the inclusion of higher-lying orbitals does not introduce any qualitative differences.

The coupling scheme in our system is demonstrated in Fig. 2. The figure shows all the possible types of coupling caused by the Coulomb interaction and FIR lasers. We use the notation $|n_x n_y n_z (elec); n_x n_y n_z (hole)\rangle$ for the determinants. The Coulomb selection rule is that the total parity is conserved. Only radiative determinants with even overall parity can be excited by an optical interband transition from an initially empty dot. For example, the radiative, even parity determinant $|211;211\rangle$ couples to the other radiative, even parity determinants $|112;112\rangle$ and $|121;121\rangle$. Further, the Coulomb interaction scatters the electron and hole into nonradiative, even parity determinants, e.g., $|111;311\rangle$. Moreover, the Coulomb interaction couples nonradiative determi-

nants to each other, e.g., $|212;112\rangle$ and $|221;121\rangle$ with $|211;311\rangle$. Hence the eigenstates of our Hamiltonian yield coupling between purely radiative determinants, between purely nonradiative determinants, or between any combination of these that conserves overall parity. These couplings lead to qualitatively different optical properties for a correlated and an uncorrelated electron-hole pair. Since the word ‘correlation’ can have many meanings, we should make clear that in this paper correlation refers to the coupling between determinants caused by the Coulomb interaction.

An FIR laser induces transfers between even parity radiative and odd parity nonradiative determinants. These odd-parity nonradiative determinants cannot be accessed optically, even with Coulomb correlations, but an FIR pulse can be used to populate them. In our model, these intersublevel transitions occur only in the x direction (Sec. II A), so the FIR changes n_x . This coupling is shown in Fig. 2 where an FIR pulse induces, for example, the transitions $|211;211\rangle \rightarrow |111;211\rangle$ and $|112;112\rangle \rightarrow |212;112\rangle$. A transfer between nonradiative determinants of different parity is also possible, for example, $|111;311\rangle \rightarrow |211;311\rangle$. Hence an optically created exciton can populate nonradiative determinants in two ways: either (i) by Coulomb scattering from radiative into nonradiative determinants with conservation of parity; or (ii) by a transfer from radiative into nonradiative components with odd parity using an FIR pulse.

C. Numerical methods

We calculate the intersublevel dipole matrix elements analytically whereas the Coulomb matrix elements are calculated numerically. At the price of an overall λ integration, the Coulomb matrix elements can be factorized into x , y , and z components using the formula $1/r = 2/\sqrt{\pi} \int_0^\infty e^{-r^2\lambda^2} d\lambda$. Each component is a function of the relevant coordinate and the variable λ . For example, the y component has an integrand of the form

$$\frac{2}{\epsilon\sqrt{\pi}} \int_0^L \int_0^L \psi_{n'_e}^*(y_e) \psi_{n'_h}^*(y_h) \times e^{-(y_e-y_h)^2\lambda^2} \psi_{n_e}(y_e) \psi_{n_h}(y_h) dy_e dy_h, \quad (5)$$

where $\psi_n(y) \sim \sin(n\pi y/L)$, and L is the lateral length. The orbitals can be expressed in complex exponential form, and Eq. (5) can be integrated with respect to y_e and y_h , reducing it to error functions with λ dependence only. There are 16 terms in Eq. (5) that are added numerically for each possible set of quantum numbers (n'_e, n'_h, n_e, n_h). The same applies to the z component. In the x direction the situation is more complicated. The orbitals have sinusoidal behavior in the wells, but a hyperbolic sine or a hyperbolic cosine behavior in the barrier. Therefore we found it easiest to integrate the x component numerically rather than follow the steps for the lateral components. Finally, the three components are multiplied and integrated numerically with respect to λ .

The correlations are treated within the framework of the time-dependent configuration interaction method.^{55,56} The total wave function $|\Psi(t)\rangle$ is expressed as a linear combina-

tion of the Slater determinants $|i\rangle$: $|\Psi(t)\rangle = \sum_i c_i(t) |i\rangle$. In our model, each $|i\rangle$ is derived from Eq. (4) and is a product of electron and hole orbitals, but we still refer to $|i\rangle$ as a determinant. We numerically propagate the time-dependent Schrödinger equation with the Hamiltonian in Eq. (1) using the Taylor expansion method proposed by Mercouris *et al.*,⁵⁷ with convergence being obtained with four to six terms in the Taylor expansion with respect to the time step. The time-propagation including the screened Coulomb interaction and a sequence of laser pulses simulates the dynamics of the single exciton. We begin with an empty dot and use an NIR pulse to create the exciton. This is followed by sequences of FIR pulses to produce different population transfers. The optical properties are analyzed in terms of the time-dependent probabilities of the dominant determinants. Previous work used this method to study exciton and biexciton correlation effects in a single GaAs quantum dot.^{5,6} The current work extends those studies to a dot with an internal tunneling barrier.

D. Variation of determinantal coefficients with splitting

The Coulomb coupling between the determinantal components of an eigenstate can be tuned by changing the dot dimensions. This is because the components have different geometrical properties besides having different optical properties. For example, $|211;211\rangle$ is most sensitive to the barrier width, $|112;112\rangle$ (or $|121;121\rangle$) is most sensitive to the length in z (or y), and $|111;311\rangle$ is most sensitive to the length in x . Sensitivity here refers to how much the energy of a determinant changes with respect to the energy of the lowest determinant $|111;111\rangle$ as the different dimensions vary. The geometrical properties of higher excitations are more complicated. Components like $|212;212\rangle$, for example, are sensitive to both the barrier width and the length in z . By changing the dot dimensions, we can control the coupling strength between the different determinants of an eigenstate. Since molecular beam epitaxy can be used to grow dots by monolayers it is feasible to control the barrier width on a subnanometer level.

As the barrier width increases from 1.4 to 4 nm, the electron splitting decreases from 52 to 22 meV. Since the splitting of the hole levels is smaller due to its larger mass, the exciton splitting is dominated by that of the electron levels. The change in splitting leads to a variation in the correlation coupling between the determinants, which in turn changes the magnitudes of the determinantal coefficients in the eigenstates. The relative signs of the components are also important. When we coherently superpose two radiative eigenstates with an NIR pulse to produce a beating, which is a measurable signature of the correlations as explained in Sec. III, the signs of the different components determine whether constructive or destructive interference is obtained.

Figure 3 shows an example of the variation of the determinantal coefficients for an eigenstate with relative signs $|112;112\rangle + |111;311\rangle - |211;211\rangle$. We have simplified the description by not showing the $y \leftrightarrow z$ symmetry explicitly. Whenever a determinant like $|112;112\rangle$ is mentioned, it is implicitly understood that the state contains an equal ampli-

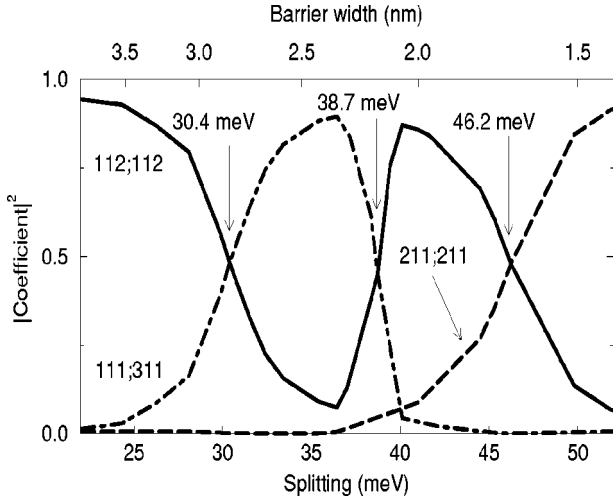


FIG. 3. Variation of determinantal coefficients with barrier width and electron splitting for an eigenstate with relative signs $|112;112\rangle + |111;311\rangle - |211;211\rangle$. The $|112;112\rangle$ probability is doubled to incorporate the $|121;121\rangle$ probability, which is not shown. At 30.4 meV (barrier width 2.8 nm) and at 38.7 meV (barrier width 2.2 nm), $|112;112\rangle$ and $|111;311\rangle$ are equally strongly correlated and have equal amplitudes. At 46.2 meV (barrier width 1.7 nm), $|112;112\rangle$ and $|211;211\rangle$ are equally strongly correlated.

tude of $|112;112\rangle$ and $|121;121\rangle$. At an electron splitting of 30.4 meV (barrier width 2.8 nm) and 38.7 meV (barrier width 2.2 nm), the $|112;112\rangle$ and $|111;311\rangle$ determinants have equal amplitudes. That is, these determinants are maximally correlated at these splittings. Another example of a strong correlation is at 46.2 meV (barrier width 1.7 nm) where $|112;112\rangle$ and $|211;211\rangle$ have equal amplitudes.

In Sec. III B, for example, we exploit the fact that another eigenstate with relative signs $|112;112\rangle - |111;311\rangle + |211;211\rangle$ has a $|112;112\rangle$ amplitude equal to the previous-paragraph eigenstate at 30.4 meV. The reason these splittings are particularly interesting is the equal amplitudes of particular radiative components in pairs of eigenstates. Hence these splittings yield strong correlation effects when these eigenstates are coherently superposed by an NIR pulse. At other splittings these amplitudes are typically not equal. However, qualitatively similar correlation-induced optical effects can still be found by compensating differences in coupling with careful adjustments of the center frequencies and pulse widths of the laser pulses.

III. RESULTS

We present three illustrative cases of the correlation-induced optical properties of our model system for an electron-hole pair in a quantum dot with an internal tunneling barrier. Cases I and II show how a correlation-induced coherent beating between determinants in two optically excited exciton states can be transferred to dark states by FIR pulses. Case III shows that even fairly weak correlations lead to new pathways for the FIR transitions.

In case I, we show that a coherent beating can be modulated with an FIR pulse. When we attempt to transfer a beat-

ing between two determinants in two radiative eigenstates into a single dark eigenstate with an FIR pulse the beating becomes modulated. However, the coherent optical excitation is not transferred into the dark eigenstate. In case II, a pair of radiative and a pair of nonradiative eigenstates are coupled by FIR pulses. Using two FIR pulses with appropriate frequencies and bandwidths, we show that a beating can be transferred unchanged back and forth between the pairs of eigenstates. This case is an unusual optical effect which shows that optical coherence created by a short NIR pulse can be transferred into a pair of dark states by an FIR pulse. As explained below, the correlations in the system ensure that pairs of radiative and dark states naturally occur. This kind of transfer opens up the possibility of optically probing coherence properties of dark eigenstates. Case III is an example of how correlation provides new optical pathways for the FIRs to perform population transfers that are not allowed without correlations. In the example we choose to discuss, FIR lasers polarized in x are used to transfer an excitonic excitation between the x direction and the lateral y, z directions. Such a directional change cannot be affected by an x -polarized FIR alone without help of the correlations. Finally, in Sec. III D, we suggest an experimental way to probe the transfer described in case III.

A. Case I: Modulated coherent beatings

In our previous work, we show that correlations in quantum dots can be optically manifested by coherent excitation of pairs of eigenstates by subpicosecond laser pulses. Due to the optical selection rules, this approach probes the coherence properties only of radiative even parity states. The strongest correlation-induced effects are then due to the Coulomb coupling between radiative and nonradiative even-parity determinants.^{5,6} In the present work we discuss how FIR's can be used to extend this approach to dark states via transfers between even and odd parity states.

This first case shows that a single dark state can modulate the coherent beating of the radiative pair, through conventional Rabi oscillations, but that very little of the coherent beating is transferred to the dark state. The pulse scheme for producing modulated beatings is shown in Fig. 4. The barrier width is 1.7 nm, at which the upper radiative (UR) and lower radiative eigenstate (LR) have equal $|211;211\rangle$ coefficients.

An NIR pulse (Table I) with a bandwidth of the order of the energy separation of LR and UR creates an exciton into a coherent superposition of these eigenstates. As shown in Fig. 5, the superposition leads to a beating in the probabilities of their radiative determinants. The $|112;112\rangle$ and $|211;211\rangle$ components undergo beating since due to correlation both determinants exist in both the radiative eigenstates (Table II). The beating frequency equals the energy difference between UR and LR. Only the $|211;211\rangle$ beating is shown in Fig. 5 since we are interested in excitations along x . The times at which the probability is zero are the times at which the $|211;211\rangle$ components of UR and LR cancel each other. Since they have equal coefficients, they give equal weights when the center frequency is placed midway between UR and LR. Otherwise, the $|211;211\rangle$ weights of the two eigen-

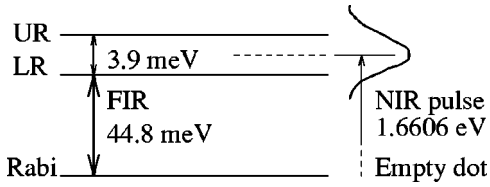


FIG. 4. Pulse scheme for producing modulated beatings at a barrier width of 1.7 nm. The determinantal compositions of the eigenstates are given in Table II, which shows equal $|211;211\rangle$ coefficients for the upper radiative (UR) and lower radiative eigenstate (LR). On the right, the bandwidth and center frequency of the NIR pulse are shown. The NIR pulse overlaps UR and LR, with center frequency midway between UR and LR, creating an exciton into a coherent superposition of these eigenstates that leads to a beating that oscillates down to zero. A FIR field with center frequency 44.8 meV drives the system into the nonradiative (Rabi) eigenstate which yields modulated beatings (Fig. 5).

states would be unequal and the beating would not oscillate down to zero. In fact, even if the coefficients are considerably different, one can still achieve zeros in the beating. For example, at 1.4-nm barrier width, LR and UR have the $|211;211\rangle$ coefficients 0.26 and 0.96, respectively. With a proper pulse center frequency, a beating which oscillates down to zero could still be achieved.

The FIR field puts the system periodically into a dark eigenstate, denoted “Rabi” in Fig. 5, causing the probability maximum of the $|211;211\rangle$ beating to be modulated. The FIR field changes the electron quantum number n_x in driving the $|211;211\rangle$ beating into the dark eigenstate with a dominant $|111;211\rangle$ component. Before the application of the FIR field, the $|211;211\rangle$ probability would oscillate between zero and a constant maximum. But now this maximum is no longer constant, it decreases and reaches a minimum when the Rabi curve is maximum and vice versa. The probability maximum of the beating is modulated. The modulation frequency, which is the Rabi frequency, is proportional to the FIR field strength.^{58–60} The Rabi oscillation period (14 ps) is slow relative to the $|211;211\rangle$ beating period (1.0 ps). Consequently, the beating is only modulated and is not transferred into the Rabi state. The large oscillations in the radiative states produce only small intensity-dependent oscillations on the Rabi curve.

In the situation discussed above and illustrated in Fig. 5, the FIR field is resonant with LR and hence off resonance with UR. The FIR therefore drives the LR population into the Rabi state with a resonant Rabi frequency $\Omega_{\text{Rabi}}^{\text{LR}}$ proportional to the FIR field strength E_{FIR} and the dipole moment

TABLE I. Parameters of the NIR and FIR pulses in the excitation scheme of Fig. 4. The duration is the full width at half maximum. The bandwidth of the pulse is 3.1 meV full width at half maximum.

Pulse	Frequency (eV)	Duration (ps)
NIR	1.661	0.81
FIR	0.045	long

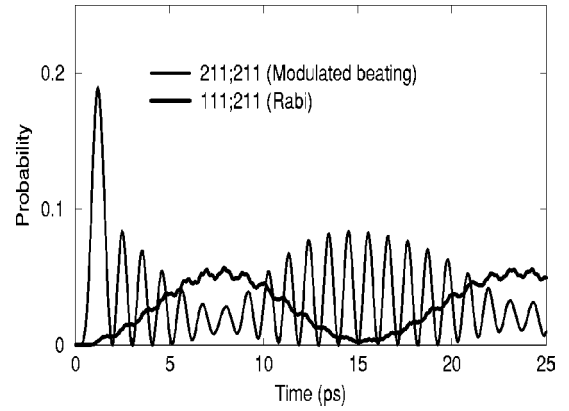


FIG. 5. Time-dependent probabilities of the radiative $|211;211\rangle$ and nonradiative (Rabi) determinant $|111;211\rangle$ for the excitation scheme in Fig. 4. The zeros of the beating correspond to times at which the radiative components cancel each other. A FIR field drives the population into the Rabi determinant. The maximum of the beating is modulated and reaches a minimum when the Rabi curve is maximum and vice versa. The modulation frequency, the Rabi frequency, is proportional to the FIR field strength.^{58–60} The beating is only modulated and is not transferred into the Rabi state except for a small, intensity-dependent variation.

D_{intersub} between the $|211;211\rangle$ and $|111;211\rangle$ determinants. That is, $\Omega_{\text{Rabi}}^{\text{LR}} = D_{\text{intersub}} E_{\text{FIR}}/2$. At the same time, the population of UR is driven into the Rabi state with an off-resonant Rabi frequency $\Omega_{\text{Rabi}}^{\text{UR}} = \sqrt{\Delta^2 + (D_{\text{intersub}} E_{\text{FIR}}/2)^2}$, where Δ is the resonance detuning between the FIR and UR. Such off-resonant Rabi oscillations are incomplete in the sense that the population of UR is never fully depleted. The amplitude of this off-resonant transfer is to first order proportional to the FIR field strength, which gives rise to the small beating on the Rabi curve. In a more symmetric situation with the FIR centered between the states UR and LR, the beatings on the Rabi curve can become stronger relative to the total amplitude in the Rabi state. But in that case both populations are driven into the Rabi state by off-resonant Rabi oscillations, which causes both transfers to be incomplete and intensity dependent.

B. Case II: Transfer of coherent beatings between paired states

Because of the correlations and a suitably chosen barrier splitting, we can find pairs of radiative and pairs of nonradiative

TABLE II. Determinantal compositions and energies of the eigenstates in Fig. 4. The barrier width is 1.7 nm, for which the radiative eigenstates have equal $|211;211\rangle$ coefficients. The $y \leftrightarrow z$ symmetry is not shown explicitly. For example, whenever a determinant like $|112;112\rangle$ is shown, it is implicitly understood that the state contains an equal amplitude of $|112;112\rangle$ and $|121;121\rangle$. Determinants with coefficients below 0.2 have been omitted.

Eigenstate	Energy (eV)	$ 112;112\rangle$	$ 111;211\rangle$	$ 211;211\rangle$
Lower radiative	1.659 eV	0.49	0.00	0.70
Upper radiative	1.663 eV	0.49	0.00	-0.70
Dark	1.614 eV	0.00	0.99	0.00

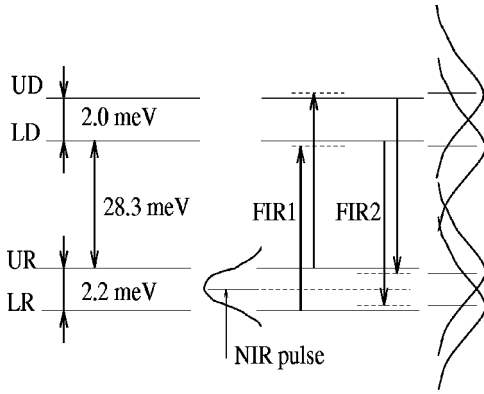


FIG. 6. Pulse scheme for transferring beatings between pairs of radiative (UR and LR) and pairs of dark eigenstates (UD and LD). The pulse parameters are given in Table III. The barrier width is 2.8 nm, and the determinantal compositions of the eigenstates are given in Table IV. The energy separation of UR and LR is not exactly equal to that of UD and LD. Therefore, as discussed in the text, to achieve equal coupling between LR and LD and between UR and UD, the FIR frequencies are shifted somewhat off resonance. The FIR pulse shapes shown to the right depict the pulse widths and their locations with respect to the energy levels. FIR1 and FIR2 have the same parameters.

ative eigenstates between which a beating can be transferred. Figure 6 shows the pulses used (Table III) for a set of eigenstates at a 2.8-nm barrier width, and Fig. 7 shows the time-varying probabilities of the dominant determinants. The determinantal compositions are given in Table IV. The $|112;112\rangle$ components of the radiative pair (UR and LR) have equal coefficients. To obtain zeros in the radiative beating, the NIR pulse is placed midway between LR and UR. To transfer the radiative beating into a dark beating, a short-duration FIR (FIR1) is used. The $|212;112\rangle$ components of the dark pair (UD and LD) are fairly close but not equal. Moreover, the energy separation of UR and LR is not exactly equal to that of UD and LD.

To make the transfer complete, equal coupling from UD and LD is ensured by shifting the FIR1 center frequency somewhat off resonance so that a balanced coupling is obtained. Due to the wide spectral width, FIR1 depopulates LR into both LD and UD, although predominantly into LD. Similarly, FIR1 depopulates UR mainly into UD but also into LD. Despite this complex situation, it is not hard to find a center frequency at which the perfect beating in the radiative pair is completely transferred into a perfect beating in the dark pair. The radiative beating is restored using a second short-duration FIR (FIR2), where FIR1 and FIR2 have the same parameters.

TABLE III. Parameters of the NIR and FIR pulses in the excitation scheme of Fig. 6. The duration is the full width at half maximum. FIR2 has the same parameters as FIR1.

Pulse	Frequency (eV)	Duration (ps)
NIR	1.692	1.1
FIR1, FIR2	0.0304	0.48

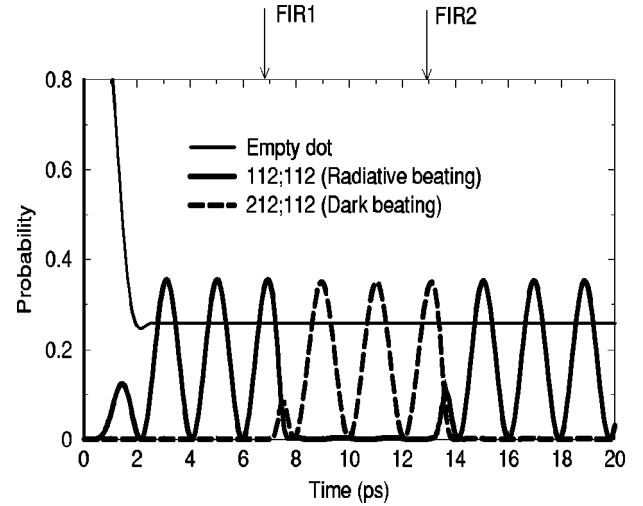


FIG. 7. Time-dependent probabilities of the radiative $|112;112\rangle$ determinant and dark $|212;112\rangle$ determinant for the excitation scheme in Fig. 6. The $|221;121\rangle$ and $|121;121\rangle$ probabilities are not shown but are exactly equal to the $|212;112\rangle$ and $|112;112\rangle$ probabilities, respectively. Two short-duration FIR's (Table III) are used to transfer the radiative beating into and out of the dark states. The radiative beating is transferred into a dark beating with FIR1. The frequency of the radiative beating equals the energy difference between UR and LR, and the frequency of the dark beating equals the energy difference between UD and LD. FIR2 restores the initial radiative beating.

This kind of transfer of coherence from an optically created exciton into a dark exciton and back again opens the possibility to optically probe, for example, the decoherence mechanisms of dark states. A disruption of the perfect beating in the dark pair, would also disrupt the perfect beating in the final pair. This scheme therefore transfers the effect of interactions with the dark pair to optically observable effects in the radiative pair. The time dependence of these effects could be probed by scanning the time delay between FIR1 and FIR2.

To achieve the complete transfer into the dark beating, the LR and UR coefficient have to be fairly close to those of the LD and UD, respectively. The slight difference is compensated for by adjusting the pulse center frequencies. The pairs of radiative and dark states with corresponding determinantal coefficients are due to the Coulomb correlations and the fact that we have chosen a barrier width for which the $|112;112\rangle$ and $|111;311\rangle$ determinants have similar energies. The $|212;112\rangle$ and the $|211;311\rangle$ determinant then also have similar energies. The radiative $|112;112\rangle$ determinant is coupled to the $|111;311\rangle$ determinant, which splits the radiative eigenstate into a pair with different relative signs between these two determinants (Table IV). Raising the n_x quantum number from 1 to 2 gives a similar Coulomb coupling between $|212;112\rangle$ and $|211;311\rangle$ as there is between $|112;112\rangle$ and $|111;311\rangle$ (see Table IV). Hence the Coulomb coupling creates two pairs of states—one radiative pair and one dark pair—that have very similar coupling coefficients and can therefore be used to enable the transfer of the population between the pairs with a single FIR pulse.

TABLE IV. Determinantal compositions and energies of the eigenstates in Fig. 6 for a 2.8 nm barrier width. The pair of radiative eigenstates have equal $|112;112\rangle$ coefficients, and the dark pair have fairly close $|212;112\rangle$ coefficients. The $y \leftrightarrow z$ symmetry is not shown explicitly (see Table II). Except for the upper radiative eigenstate, determinants with coefficients below 0.2 have been omitted.

Eigenstate	Energy (eV)	$ 112;112\rangle$	$ 212;112\rangle$	$ 111;311\rangle$	$ 211;311\rangle$	$ 211;211\rangle$
Lower radiative	1.691 eV	0.49	0.00	0.70	0.00	0.00
Upper radiative	1.693 eV	0.49	0.00	-0.70	0.00	0.12
Lower dark	1.721 eV	0.00	0.44	0.00	0.76	0.00
Upper dark	1.723 eV	0.00	0.54	0.00	-0.63	0.00

C. Case III: Transfer of excitonic excitations between different directions

The transfer by an FIR laser of an excitonic excitation into a direction perpendicular to the direction of polarization of the FIR is another example of a correlation induced optical effect. This case is illustrative of the opening of new FIR pathways by the correlations. An excitation can be transferred between different directions using a scheme of one NIR and two FIR pulses. The pulse scheme is shown in Fig. 8 for a 2.8-nm barrier width, and the pulse parameters are given in Table V. Unlike the previous cases, the initial NIR pulse excites only one eigenstate. The pulse is sufficiently spectrally sharp not to overlap any nearby radiative eigenstates. The exciton is created in an initial eigenstate that has a dominant $|211;211\rangle$ component and weakly correlated $|112;112\rangle$ and $|111;311\rangle$ components (Table VI).

As shown in Fig. 9, an FIR pulse (FIR1) drives the excitonic excitation completely into the intermediate dark eigenstate, which has large $|212;112\rangle$ and $|211;311\rangle$ components. The small $|112;112\rangle$ component of the initial eigenstate provides the pathway for FIR1 to take the system into the $|212;112\rangle$ component of the intermediate eigenstate. Without that small component this transfer would not be possible since a direct $|211;211\rangle \rightarrow |212;112\rangle$ transfer violates the in-

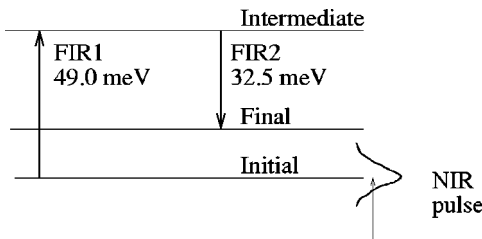


FIG. 8. Pulse scheme for performing a transfer from an initial radiative eigenstate with excitonic excitation in x to a final radiative eigenstate with excitonic excitation in y and z . The pulse parameters are given in Table V. The barrier width is 2.8 nm. The determinantal compositions of the eigenstates are given in Table VI. Table VI shows that the initial eigenstate has a dominant $|211;211\rangle$ component, and the final eigenstate has a large $|112;112\rangle$ component. The NIR pulse exciting the initial eigenstate is sharp enough not to overlap any nearby radiative eigenstates. An FIR pulse (FIR1) drives the system into an intermediate dark eigenstate. FIR2 drives the system into the final eigenstate. The radiative part of the excitation initially in x is transferred to one in y and z with two x -polarized FIR's, which transfer is not possible without correlation.

tersublevel selection rule. Similarly, there is a transfer between the $|111;311\rangle$ component of the initial eigenstate, and the $|211;311\rangle$ component of the intermediate eigenstate.

The second FIR (FIR2) drives the system into the final eigenstate with large $|112;112\rangle$ and $|111;311\rangle$ components. In effect, the radiative initial excitation $|211;211\rangle$ in x is transferred to $|112;112\rangle$ which is a radiative excitation in z (and y by symmetry). This kind of transfer is only possible with Coulomb correlations. The duration of FIR2 in Fig. 9 was chosen long enough to produce Rabi oscillations between the intermediate and final eigenstate to illustrate the resonant coupling between these two states. In contrast to beatings between dark and radiative determinants,^{5,6} the kind of directional transfer discussed here between radiative determinants is harder to probe optically. Therefore we propose in the next section a modification of this case that does lead to an optically probable effect.

D. Probing case III at optimal superposition

With some changes in the scheme presented above, a short NIR pulse can be used to probe the transfer of the excitonic excitation between different directions. With a similar pulse scheme as in Sec. III C but with different intensities and durations, a situation as the one depicted in Fig. 10 can be obtained. The difference is that the initial state is only partially depleted. We choose the FIR1 and FIR2 intensities and durations such that the total amplitudes at moments of destructive interference of $|211;211\rangle$ and $|112;112\rangle$ of the initial eigenstate exactly cancel the $|112;112\rangle$ amplitude of the final eigenstate. Since all these determinants are radiative this leads to a beating between radiative and dark character of the state at constructive and destructive interference, respectively, with a frequency equal to the energy separation of the initial and final states. At destructive interference the to-

TABLE V. Parameters of the NIR and FIR pulses in the excitation scheme of Fig. 8. The duration is the full width at half maximum. FIR1 is activated such that its amplitude is maximum at $t = 0$.

Pulse	Frequency (eV)	Duration (ps)
NIR	1.674	1.1
FIR1	0.049	7.1
FIR2	0.033	15.5

TABLE VI. Determinantal compositions and energies of the eigenstates in Fig. 8 for a 2.8-nm barrier width. The initial one has a dominant $|211;211\rangle$ component, and weakly correlated $|112;112\rangle$ and $|111;311\rangle$ components. The intermediate one has strongly correlated $|212;112\rangle$ and $|211;311\rangle$ components. The final one has strongly correlated $|112;112\rangle$ and $|111;311\rangle$ components. The $y \leftrightarrow z$ symmetry is not shown explicitly (see Table II). Except for the initial eigenstate, determinants with coefficients below 0.2 have been omitted.

Eigenstate	Energy (eV)	$ 112;112\rangle$	$ 212;112\rangle$	$ 111;311\rangle$	$ 211;311\rangle$	$ 211;211\rangle$
Initial	1.674 eV	0.10	0.00	-0.11	0.00	0.98
Intermediate	1.721 eV	0.00	0.44	0.00	0.76	0.00
Final	1.691 eV	0.49	0.00	0.70	0.00	0.00

tal wave function is optically dark. An NIR pulse with duration (0.1 ps) sufficiently shorter than that of the beating period (0.25 ps) can then be used to probe this beating in the optical response. The probe pulse center frequency is located midway between the initial and final eigenstates.

As shown in Fig. 11, by scanning the time delay of the probe pulse the beating can be manifested in the empty-dot probability, which can then be measured by some secondary optical probing. At the maximum of the $|112;112\rangle$ final-state beating in Fig. 10, electron-hole recombination is maximal as shown by the rise in the empty-dot probability curve. However, the recombination is only partial. The field strength could have been chosen to cause complete recombination but this would be accompanied by high-intensity effects. At a minimum of the beating, the equal amplitudes mentioned earlier cancel each other (destructive interference). Hence no electron-hole recombination takes place and the system is optically transparent to the probe pulse. Mathematically, the initial coefficients are multiplied by a weight-

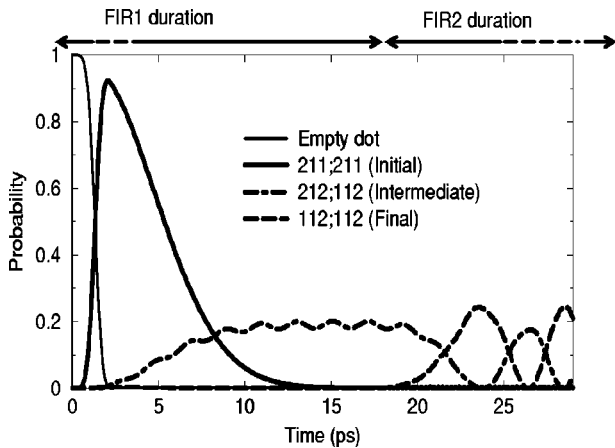


FIG. 9. Time-dependent probabilities of the radiative $|211;211\rangle$ and $|112;112\rangle$ determinants and the dark $|212;112\rangle$ determinant for the excitation scheme in Fig. 8. The $|121;121\rangle$ and $|221;121\rangle$ probabilities are not shown but are exactly equal to the $|112;112\rangle$ and $|212;112\rangle$ probabilities, respectively. The exciton optically excited into $|211;211\rangle$ of the initial eigenstate is driven by FIR1 into $|212;112\rangle$ of the intermediate dark eigenstate. FIR2 then drives the exciton into $|112;112\rangle$ of the final eigenstate. This $x \rightarrow y, z$ transfer of the excitation is not possible without correlation. The arrows indicate the duration of the FIRs. FIR1 has a maximum amplitude at $t=0$. The duration of FIR2 was chosen to show Rabi oscillations between the intermediate and final eigenstate.

ing factor $w_{initial}$, and the final ones by a weighting factor w_{final} . With the coefficients in Table VI, the probe pulse at destructive interference adds the radiative coefficients according to the equation: $0.98w_{initial} - 2(0.49w_{final} - 0.10w_{initial})$ such that it yields zero. The factor 2 is due to the $y \leftrightarrow z$ symmetry of $|112;112\rangle$.

Some of the finer details of the dynamics in Fig. 10 can be explained in the following way. The small beating in the $|211;211\rangle$ probability of the initial state is because of an additional eigenstate (same as UR in case II, Table IV), $0.49|112;112\rangle - 0.70|111;311\rangle + 0.12|211;211\rangle$, which lies above the final one with energy 1.693 eV. It is fairly close to the final eigenstate with energy 1.691 eV, and is therefore excited by FIR2. It has a small $|211;211\rangle$ component which coherently adds to the $|211;211\rangle$ component of the initial eigenstate. Further, when the probe pulse is gone, the $|211;211\rangle$ and $|112;112\rangle$ beatings become modulated. This

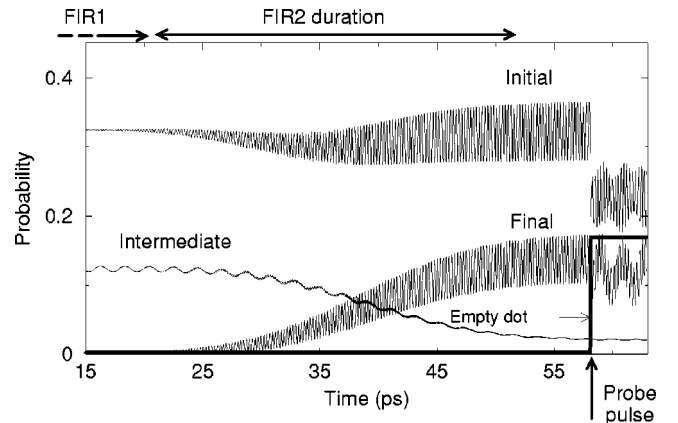


FIG. 10. Electron-hole recombination due to an NIR probe pulse. The first 15 ps of the simulation are not shown. We use the same pulse scheme as in Fig. 8. The labeling of the states is the same as in Fig. 9, but the FIR intensities and durations are different. We choose the FIR intensities and durations such that the total initial radiative amplitudes are equal to the final radiative amplitude at destructive interference, which occurs at the minimum in the oscillations of the final determinant $|112;112\rangle$. A short-duration (0.1 ps) NIR pulse can be used to probe the optical response of the system. The probe has its center frequency midway between the initial and final eigenstates. If the probe pulse arrives at destructive interference, no electron-hole recombination takes place. If the probe pulse arrives at other times, electron-hole recombination is induced. The figure shows the situation that gives maximal recombination, as indicated by the sharp rise in the empty-dot probability.

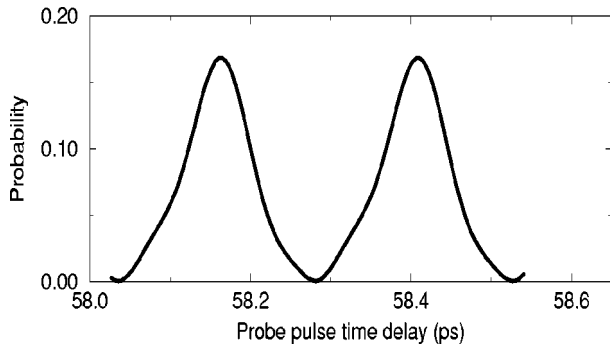


FIG. 11. Empty dot probability as a function of the NIR probe pulse time delay. This result is obtained by scanning the probe pulse over the time range of two complete beatings of the final probability curve in Fig. 10.

is because the probe pulse overlaps not just the initial and final eigenstates, but also this additional one. It is excited by the probe pulse, and since the recombination is only partial, the beatings become modulated. The modulation frequency equals the energy difference between the final and additional eigenstate.

Finally, let us stress that the main beating probed by the probe pulse and caused by the interference between the $|211;211\rangle$ and $|112;112\rangle$ components is a manifestation of correlations between these two determinants. This kind of beating cannot be obtained merely by considering the eigenstates that could be coupled by an x -polarized FIR without correlations. The fact that the dot dimensions are such that the $|211;211\rangle$ and $|112;112\rangle$ determinants have similar energies makes the pulse scheme suggested here able to uniquely probe the transfer between the $|211;211\rangle$ and $|112;112\rangle$ determinants.

IV. SUMMARY

In nanoscale semiconductor quantum dots the kinetic and Coulomb excitation energies are of the same order of magnitude. Hence there is an interplay between confinement and Coulomb correlation which can be studied using fast laser pulses. Our model is a prototypical GaAs dot with an internal AlGaAs tunneling barrier. The presence of a tunneling barrier provides the freedom of changing the level splitting along the double well without changing the outer dot dimensions. The hole mass is heavy along the growth direction, and light in the lateral directions. We treat a single exciton confined in the dot within the effective mass approximation. The Coulomb interaction couples determinants of different optical and geometrical properties, which yields interesting optical effects. These couplings can be tuned by changing the barrier width and the dot dimensions, and lead to different

optical properties between a correlated and an uncorrelated system. Radiative eigenstates, which have even parity, can be depopulated into nonradiative eigenstates of odd parity via FIR pulses. Different pulse schemes can be used to produce a variety of correlation-induced optical behavior.

By numerically propagating the time-dependent Schrödinger equation for an electron-hole pair driven by a sequence of NIR and FIR pulses, we present three illustrative cases of coherent coupling between radiative and dark states. The main purpose is to extend our previous work^{5,6} on optically manifested correlation effects among radiative eigenstates to nonradiative eigenstates, and to demonstrate how the tuning of the barrier width can optimize the effects. The first case showed that a coherent optical excitation in a pair of radiative states cannot be transferred into a single nonradiative eigenstate. This is because the time scales of the beating and the Rabi oscillation are too different, and therefore the beating is only modulated. To achieve a complete transfer into a dark beating, two nonradiative eigenstates are needed with determinantal coefficients similar to those of the radiative pair of eigenstates. Coulomb correlations and a suitably chosen barrier splitting readily create such pairs of eigenstates. We were able to achieve a complete transfer of the radiative beating into and out of a pair of dark eigenstates using short-duration FIR pulses with appropriate center frequencies.

The third case, illustrating the opening of unusual FIR pathways, is the transfer of an excitonic excitation into a direction perpendicular to the FIR polarization. An initial radiative eigenstate is transferred into an intermediate dark eigenstate with an FIR pulse, despite the fact that their dominant components violate the intersublevel selection rule. However, correlations make the transfer possible by the addition to the initial eigenstate of a small radiative component that does satisfy the selection rule. Another FIR drives the excitation from the intermediate into a final radiative eigenstate where the exciton is excited in a direction perpendicular to the direction of polarization of the FIR. Finally, we propose a modification of this case that yields an optically probable effect. The FIR intensities are chosen to ensure that the initial radiative components have a total amplitude equal to that of the final radiative component, which periodically makes the system optically transparent to a probe pulse. This interference between the stimulated recombination from the initial and final states yields a strong beating with the probe-pulse time delay of the probability to find an empty dot.

ACKNOWLEDGMENTS

This work was supported by NSF and the NCSA and OSC supercomputer centers.

¹A. Zunger, MRS Bull. **23**, 35 (1998).

²D. Bimberg, M. Grundmann, and N. N. Ledentsov, *Quantum Dot Heterostructures* (Wiley, Chichester, 1999).

³G. W. Bryant, Phys. Rev. Lett. **59**, 1140 (1987).

⁴H. Gotoh, H. Ando, and H. Kanbe, Appl. Phys. Lett. **68**, 2132 (1996).

⁵L. Jönsson, M. M. Steiner, and J. W. Wilkins, Appl. Phys. Lett. **70**, 1140 (1997).

- ⁶L. Jönsson (unpublished).
- ⁷C. F. Klingshirn, *Semiconductor Optics* (Springer, Berlin, 1995).
- ⁸G. W. Bryant, Phys. Rev. B **48**, 8024 (1993).
- ⁹G. W. Bryant, Physica B **189**, 34 (1993).
- ¹⁰A. Franceschetti, L. W. Wang, H. Fu, and A. Zunger, Phys. Rev. B **58**, 13 367 (1998).
- ¹¹A. Franceschetti, H. Fu, L. W. Lang, and A. Zunger, Phys. Rev. B **60**, 1819 (1999).
- ¹²S. Lee, L. Jönsson, J. W. Wilkins, G. W. Bryant, and G. Klimeck, Phys. Rev. B **63**, 195318 (2001).
- ¹³N. A. Hill and B. Whaley, J. Chem. Phys. **99**, 3707 (1993).
- ¹⁴N. A. Hill and B. Whaley, J. Chem. Phys. **100**, 2831 (1994).
- ¹⁵N. A. Hill and B. Whaley, Phys. Rev. Lett. **75**, 1130 (1995).
- ¹⁶K. Leung, S. Pokrant, and K. B. Whaley, Phys. Rev. B **57**, 12 291 (1998).
- ¹⁷M. Grundmann, O. Stier, and D. Bimberg, Phys. Rev. B **52**, 11 969 (1995).
- ¹⁸U. Banin, J. C. Lee, A. A. Guzelian, A. V. Kadavanich, A. P. Alivisatos, W. Jaskolski, G. W. Bryant, Al. L. Efros, and M. Rosen, J. Chem. Phys. **109**, 2306 (1998).
- ¹⁹L.-W. Wang and A. Zunger, Phys. Rev. Lett. **73**, 1039 (1994).
- ²⁰L.-W. Wang and A. Zunger, Phys. Rev. B **53**, 9579 (1996).
- ²¹L. Landin, M.-E. Pistol, C. Pryor, M. Persson, L. Samuelson, and M. Miller, Phys. Rev. B **60**, 16 640 (1999).
- ²²A. J. Williamson and A. Zunger, Phys. Rev. B **61**, 1978 (2000).
- ²³L. M. Ramaniah and S. V. Nair, Phys. Rev. B **47**, 7132 (1993).
- ²⁴R. Ugajin, Phys. Rev. B **51**, 11 136 (1995).
- ²⁵C. H. Sikorski and U. Merkt, Phys. Rev. Lett. **62**, 21 614 (1989).
- ²⁶D. A. Broido, K. Kempa, and P. Bakshi, Phys. Rev. B **42**, 11 400 (1990).
- ²⁷M. Grundmann, N. N. Ledentsov, O. Stier, D. Bimberg, V. M. Ustinov, P. S. Kop'ev, and Zh. I. Alferov, Appl. Phys. Lett. **68**, 979 (1996).
- ²⁸D. Gammon, E. S. Snow, B. V. Shanabrook, D. S. Katzer, and D. Park, Phys. Rev. Lett. **76**, 3005 (1996).
- ²⁹D. Gammon, E. S. Snow, B. V. Shanabrook, D. S. Katzer, and D. Park, Science **273**, 87 (1996).
- ³⁰D. Hessman, P. Castrillo, M.-E. Pistol, and L. Samuelson, Appl. Phys. Lett. **69**, 749 (1996).
- ³¹N. H. Bonadeo, J. Erland, D. Gammon, D. Park, D. S. Katzer, and D. G. Steel, Science **282**, 1473 (1998).
- ³²L. Landin, M. S. Miller, M.-E. Pistol, C. E. Pryor, and L. Samuelson, Science **280**, 262 (1998).
- ³³P. P. Paskov, P. O. Holtz, B. Monemar, J. M. Garcia, W. V. Schoenfeld, and P. M. Petroff, Appl. Phys. Lett. **77**, 812 (2000).
- ³⁴S. Fafard, Z. R. Wasilewski, C. Ni. Allen, D. Picard, M. Spanner, J. P. McCaffrey, and P. G. Piva, Phys. Rev. B **59**, 15 368 (1999).
- ³⁵S. Fafard, Z. R. Wasilewski, C. Ni. Allen, D. Picard, P. G. Piva, and J. P. McCaffrey, Superlattices Microstruct. **25**, 87 (1999).
- ³⁶H. C. Liu, M. Gao, J. McCaffrey, Z. R. Wasilewski, and S. Fafard, Appl. Phys. Lett. **78**, 79 (2001).
- ³⁷F. Heinrichsdorff, M. Grundmann, O. Stier, A. Krost, and D. Bimberg, J. Cryst. Growth **195**, 540 (1998).
- ³⁸S. Fafard, M. Spanner, J. P. McCaffrey, and Z. R. Wasilewski, Appl. Phys. Lett. **76**, 2268 (2000).
- ³⁹P. Boucaud, K. S. Gill, J. B. Williams, M. S. Sherwin, W. V. Schoenfeld, and P. M. Petroff, Appl. Phys. Lett. **77**, 510 (2000).
- ⁴⁰P. Boucaud, J. B. Williams, K. S. Gill, M. S. Sherwin, W. V. Schoenfeld, and P. M. Petroff, Appl. Phys. Lett. **77**, 4356 (2000).
- ⁴¹S. Sauvage, P. Boucaud, J.-M. Gérard, and V. Thierry-Mieg, Phys. Rev. B **58**, 10 562 (1998).
- ⁴²S. Sauvage, P. Boucaud, F. Glotin, R. Prazeres, J.-M. Ortega, A. Lemaitre, J.-M. Gérard, and V. Thierry-Mieg, Phys. Rev. B **59**, 9830 (1999).
- ⁴³S. V. Gaponenko, *Optical Properties of Semiconductor Nanocrystals* (Cambridge University Press, Cambridge, England, 1998).
- ⁴⁴C. Weisbuch and B. Vinter, *Quantum Semiconductor Structures* (Academic Press, Boston, 1991).
- ⁴⁵J. H. Davies, *The Physics of Low-Dimensional Semiconductors* (Cambridge University Press, Cambridge, England, 1998).
- ⁴⁶P. K. Basu, *Theory of Optical Processes in Semiconductors* (Clarendon, Oxford, 1997).
- ⁴⁷*Semiconductors—Basic Data*, edited by O. Madelung (Springer, Berlin, 1996).
- ⁴⁸N. W. Ashcroft and N. D. Mermin, *Solid State Physics* (Saunders College, Philadelphia, 1988).
- ⁴⁹S. Gwo, K.-J. Chao, and K. Shih, Phys. Rev. Lett. **71**, 1883 (1993).
- ⁵⁰U. Ekenberg, Phys. Rev. B **36**, 6152 (1987).
- ⁵¹H. C. Casey, Jr. and M. B. Panish, *Heterostructure Lasers* (Academic Press, New York, 1987).
- ⁵²W. H. Press, S. A. Teukolsky, W. T. Vetterling, and B. P. Flannery, *Numerical Recipes in C* (Cambridge University Press, New York, 1999).
- ⁵³K. Brunner, G. Abstreiter, G. Böhm, G. Tränkle, and G. Weimann, Phys. Rev. Lett. **73**, 1138 (1994).
- ⁵⁴G. Bastard, *Wave Mechanics Applied to Semiconductor Heterostructures* (Halsted Press, Wiley, New York, 1988).
- ⁵⁵A. Szabo and N. S. Ostlund, *Modern Quantum Chemistry* (McGraw-Hill, New York, 1989).
- ⁵⁶Y. Z. Hu, M. Lindberg, and S. W. Koch, Phys. Rev. B **42**, 1713 (1990).
- ⁵⁷Th. Mercouris, Y. Komninos, S. Dionissopoulou, and C. A. Nicolaides, Phys. Rev. A **50**, 4109 (1994).
- ⁵⁸C. Cohen-Tannoudji, B. Diu, and F. Laloë, *Quantum Mechanics* Vol. I (Wiley, New York, 1977).
- ⁵⁹L. Allen and J. H. Eberly, *Optical Resonance and Two-Level Atoms* (Dover, New York, 1987).
- ⁶⁰J. J. Sakurai, *Modern Quantum Mechanics* (Addison Wesley, Reading, MA, 1994).